Earth **Surface**
Dynamics

Using a calibrated upper living position of marine biota to calculate coseismic uplift: a case study of the 2016 Kaikōura earthquake, New Zealand

Catherine Reid[1], John Begg[2], Vasiliki Mouslopoulou[3,4], Onno Oncken[4], Andrew Nicol[1], and Sofia-Katerina Kufner[4,5]

[1]School of Earth and Environment, University of Canterbury,
Private Bag 4800, Christchurch, 8140, New Zealand
[2]GNS Science, P.O. Box 30-368, Lower Hutt, New Zealand
[3]National Observatory of Athens, Institute of Geodynamics, Lofos Nimfon, Athens, 11810, Greece
[4]GFZ Helmholtz Centre Potsdam, German Research Centre for Geosciences,
Telegrafenberg, 14473 Potsdam, Germany
[5]British Antarctic Survey, High Cross, Madingley Rd, Cambridge, CB3 0ET, UK

Correspondence: Vasiliki Mouslopoulou (vasiliki.mouslopoulou@noa.gr)

Abstract. The 2016 $M_w = 7.8$ Kaikōura earthquake (South Island, New Zealand) caused widespread complex ground deformation, including significant coastal uplift of rocky shorelines. This coastal deformation is used here to develop a new methodology, in which the upper living limits of intertidal marine biota have been calibrated against tide-gauge records to quantitatively constrain pre-deformation biota living position relative to sea level. This living position is then applied to measure coseismic uplift at three other locations along the Kaikōura coast. We then assess how coseismic uplift derived using this calibrated biological method compares to that measured using other methods, such as light detection and ranging (lidar) and strong-motion data, as well as non-calibrated biological methods at the same localities. The results show that where biological data are collected by a real-time kinematic (RTK) global navigation satellite system (GNSS) in sheltered locations, this new tide-gauge calibration method estimates tectonic uplift with an accuracy of $\pm \leq 0.07$ m in the vicinity of the tide gauge and an overall mean accuracy of ± 0.10 m or 10 % compared to differential lidar methods for all locations. Sites exposed to high wave wash, or data collected by tape measure, are more likely to show higher uplift results. Tectonic uplift estimates derived using predictive tidal charts produce overall higher uplift estimates in comparison to tide-gauge-calibrated and instrumental methods, with mean uplift results 0.21 m or 20 % higher than lidar results. This low-tech methodology can, however, produce uplift results that are broadly consistent with instrumental methodologies and may be applied with confidence in remote locations where lidar or local tide-gauge measurements are not available.

1 Introduction

Vertical displacement has been measured globally using intertidal marine biota on rocky coastlines, which often provide important constraints for incremental uplift during large-magnitude earthquakes and cumulative geological uplift (e.g. Alaska: Plafker, 1965; California: Carver et al., 1994; Mexico: Bodin and Klinger, 1986; Ramirez-Herrera and Orozco, 2002; Costa Rica: Plafker and Ward, 1992; Chile: Fitzroy, 1839; Castilla, 1988; Castilla et al., 2010; Farías, 2010; Vargas et al., 2011; Melnick et al., 2012; Argentina: Ortlieb et al., 1996; eastern Mediterranean: Pirazzoli et al., 1982; Stiros et al., 1992; Laborel and Laborel-Dugeun, 1994; Mouslopoulou et al., 2015a; Japan: Pirazzoli et al., 1985; New Zealand: Mouslopoulou et al., 2019). Biological data were the basis for the first written records of coastal uplift following earthquakes along the Chilean coast (Graham, 1824; Fitzroy, 1839; Wesson, 2017) and continue to provide important constraints for elastic rebound and coseismic slip processes together with the locations, depth and dip of causal faults (e.g. Melnick et al., 2012; Wesson et al., 2015; Mouslopoulou et al., 2015b, 2019).

Biological indicators such as lithophagid borings and stranded bioconstructions of corals, coralline algae and barnacles, along with brown algae, gastropods, bivalves and additional intertidal species with locally reliable tidal elevation zones, have been used to estimate eustatic sea level changes and rock uplift (or subsidence) due to tectonic processes (Laborel and Laborel-Dugeun, 1994). Quantifying earthquake uplift from such biological datasets has been achieved using a variety of techniques from simple measuring devices, such as tape measures, to laser survey methods and global navigation satellite system (GNSS) techniques. While some studies (e.g. Melnick et al., 2012; Jaramillo et al., 2017) have successfully compared the reliability of the conventionally acquired biological uplift records against real-time kinematic (RTK) global navigation satellite system (GNSS) measurements, none have attempted to numerically and independently quantify the living position of each biological marker. Jaramillo et al. (2017) compare pre- and post-deformation intertidal biota, but most studies, including this one, rely on post-deformation data only. Clark et al. (2017) and Mouslopoulou et al. (2019) use a variety of methods to record deformation immediately following the 2016 Kaikōura earthquake; however, their marine biota measurements have not previously been calibrated. Moreover, none of the above studies have systematically compared the manually collected tape-measure estimates of coseismic uplift with instrumental earthquake uplift datasets at individual localities to quantitatively assess the potential uncertainty inherent in the various techniques.

In this paper we use uplift produced by the 14 November 2016 $M_w = 7.8$ Kaikōura earthquake (South Island, New Zealand) to develop a methodology for calibrating coastal vertical deformation utilising the displacement of biological marker horizons near a local tide-gauge site. This calibrated information can then be applied to estimating coastal uplift or subsidence at other sites in the Kaikōura region. Capitalising on the long-term, continuous, high-precision tide-gauge readings at Kaikōura Peninsula, biological markers within the intertidal zone uplifted during the earthquake are here utilised to (a) develop a new methodology with which to independently calculate (and thus calibrate) the upper living position of individual intertidal (algal) taxa (organisms which are widely used to measure coseismic vertical displacement) and (b) compare, at each of three localities, the conventional biologically constrained handheld measurements of coseismic uplift to values derived using various real-time remote sensing and other instrumental techniques, such as RTK GNSS, lidar and strong-motion seismometers. The results may have applications to inform future studies of the reliability of biological uplift measurements along rocky shores arising from large earthquakes at mid-latitudes (particularly in the Southern Hemisphere) and with moderate tidal ranges (e.g. ∼ 2 m), especially where instrumental technologies, such as differential lidar, are not available.

2 Geological and biological setting

2.1 The 2016 Kaikōura earthquake

The 2016 $M_w = 7.8$ Kaikōura earthquake ruptured across the southern end of the Hikurangi subduction margin in the northeastern South Island of New Zealand (Mouslopoulou et al., 2019). Northeast of the Kaikōura earthquake surface rupture, the plate boundary is dominated by oblique subduction of the Pacific Plate beneath the Australian Plate at rates of 40–47 mm yr^{-1} (De Mets et al., 1994) (Fig. 1, inset). At the southern termination of the subduction, relative plate motion is transferred onto the transcurrent Alpine Fault via strike-slip on the Marlborough Fault System (MFS) (Pondard and Barnes, 2010; Wallace et al., 2012). The MFS generally strikes parallel to the relative plate motion vector, and these active faults mainly accommodate right-lateral strike-slip with the amount of fault-related uplift increasing towards the coast. Offshore and east of the surface rupture, plate boundary deformation manifests itself as an accretionary prism complex. The accretionary complex and eastern MFS are underlain by the Pacific Plate which, based on the presence of a Wadati–Benioff zone, extends to a depth of at least 200 km beneath the northern South Island (Eberhart-Phillips and Bannister, 2010). The subducting slab is at a depth of ∼ 20–30 km beneath the surface fault traces at Kaikōura (Nicol et al., 2018) and ruptured in response to slip triggered by these surface-breaking faults during the earthquake (Mouslopoulou et al., 2019).

The Kaikōura earthquake is the largest ($M_w = 7.8$) historic earthquake to have ruptured within the southern termination of the Hikurangi subduction margin (Mouslopoulou et al., 2019). The earthquake involved a complex network
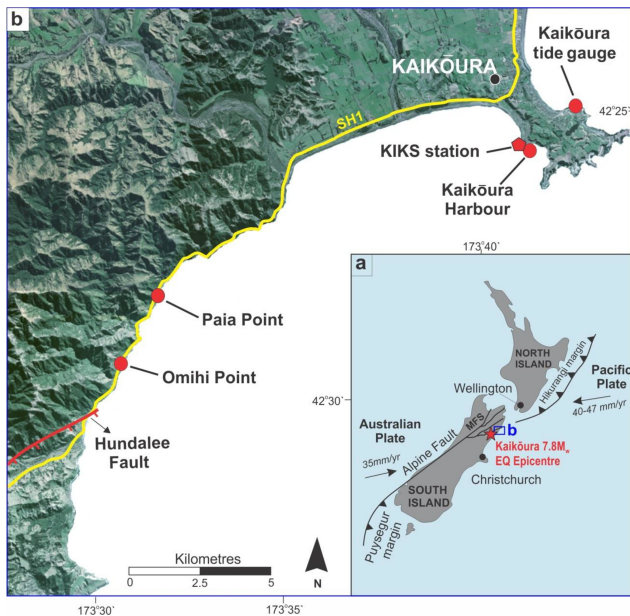
Figure 1. (a) Inset map of New Zealand illustrating the main tectonic features of the Hikurangi subduction margin, the location of the Marlborough Fault System (MFS) and the epicentre of the 2016 $M_w = 7.8$ Kaikōura earthquake. The blue box near the Kaikōura earthquake epicentre indicates the study area. **(b)** Map showing the study localities from which *Durvillaea* and *Carpophyllum* holdfast measurements were recorded using RTK GNSS and tape measure, the position of State Highway 1 (SH1) from which lidar data points were derived (see yellow line), the location of the Kaikōura tide gauge, and the KIKS strong-ground-motion station. The Hundalee Fault is also located. The background image is supplied by Land Information New Zealand.

of at least 21 strike-slip, thrust and oblique-slip upper-plate faults that ruptured the ground surface and straddle the coastline of the northeast South Island (Hamling et al., 2017; Litchfield et al., 2018). The event's complexity is reflected in the moment tensor of the main shock, which features only 65 % to 75 % double-couple percentage (GEOFON; http://geofon.gfz-potsdam.de, last access: 20 March 2017) and is characterised by an oblique mechanism with components of thrusting and right-lateral slip. Fault ruptures generally propagated northwards from the epicentre for about 200 km, with a focal depth of the main shock at 15 km (Hamling et al., 2017; Kaiser et al., 2017; Cesca et al., 2017). The resulting surface ruptures vary in strike from east–west to north-northwest, with the faults having east-northeast strike being primarily right-lateral strike-slip and more northerly striking faults accommodating strike-slip and reverse displacement (Nicol et al., 2018). The earthquake ruptured three faults (Hundalee, Papatea and Kekerengu faults) that cross the coastline and locally produced differential uplift of the rocky shorelines. Vertical displacement of −0.5 to +8 m occurred along > 100 km of coastline, with the highest values in the hanging wall of the reverse sinistral Papatea Fault north

of Kaikōura (Litchfield et al., 2018; Mouslopoulou et al., 2019). The coastal section examined in this paper is crossed by the Hundalee Fault (Fig. 1; see also Fig. 1c in Mouslopoulou et al., 2019), which accommodated a component of reverse displacement and uplift of the coast up to ∼ 2 m. In addition to the mapped surface faults, the spatial extent of coastal uplift, the widespread occurrence of tsunamis (which propagated for distances of up to ∼ 250 km from Kaikōura south; Power et al., 2017) and the significant after-slip on the plate interface suggest that faulting at the ground surface was accompanied by slip on the subduction interface and an offshore thrust fault that splays from the plate interface to extend within the accretionary prism complex (e.g. Cesca et al., 2017; Mouslopoulou et al., 2019).

2.2 Physical and biological setting

The northern Canterbury coastline is predominantly exposed to wave action, strikes northeast–southwest and is broken only by the promontory of the Kaikōura Peninsula (Fig. 1). Hinterland topography is steep and the coastal strip is narrow, comprising mainly greywacke bedrock beneath bouldery shorelines interrupted by bays with gravel-dominated beaches. Prevailing winds from the northeast (summer months) and southwest (winter months) maintain year-round exposure, and the coastline supports biota adapted to this high-energy setting. The region is in a cool temperate oceanographic setting with semi-diurnal tides with a daily tidal variation of ∼ 2 m. These factors influence the living positions of intertidal biota.

The intertidal biota in this cool temperate setting is dominated by seaweeds, typically the large brown algae *Durvillaea antarctica* (bull kelp), *D. willana*, *Carpophyllum maschalocarpum* (Fig. 2a), and *Hormosira banksii*, coralline algae (Fig. 2b), barnacles, limpets, chitons and mobile invertebrates (Marsden, 1985). Attached invertebrates, such as mussels and oysters, are present but not common on this stretch of coast. On the Kaikōura Peninsula species diversity is high, with up to 78 species present in a single intertidal transect (Marsden, 1985). The vertical distribution of species on these rocky shores is controlled by exposure to wave action and interspecies competition (Sharyn Goldstien, personal communication, 2017). The rocky shores around Kaikōura support three major biozones that approximately correspond to tidal height: (a) an upper belt of littorinid gastropods (e.g. *Littorina unifasciata* and *L. cincta*) and barnacles (e.g. *Epopella plicata*); (b) a mid-tidal region dominated by grazing molluscs (e.g. *Cellana denticulata*, *Melagraphia aethiops* and *Turbo smaragdus*); and (c) a lower zone of brown algae (e.g. *Durvillaea antarctica* and *Carpophyllum maschalocarpum*) (Marsden, 1985). When the shoreline was inspected about 2.5 months after earthquake uplift, many mobile taxa were absent in the uplifted intertidal zone, and living or dead remains of stranded encrusting or attached taxa, such as barnacles, coralline algae and brown algae, dominated the

shoreline. The green alga *Ulva* is normally present in limited amounts (Marsden, 1985); however, following the Kaikōura earthquake and shoreline disturbance, growth of this alga was prolific and it subsequently covered much of the post-earthquake intertidal zone in the study area (Fig. 2b–d). This proliferation was accompanied by the death and bleaching of stranded coralline red algae, forming a distinctive white crust on rocky surfaces (Fig. 2b and d) which was often visible at kilometre-scale distances; at that time, this was the most obvious visual indicator of uplift along the coastline.

In this study the brown algae *Durvillaea* and *Carpophyllum* are utilised to measure coastal uplift. *Durvillaea* is restricted to the Southern Hemisphere and occurs on rocky coastlines throughout New Zealand, while *Carpophyllum* is endemic (Adams, 1994). Around the Kaikōura Peninsula and north Canterbury coast, holdfasts of *Durvillaea antarctica* (bull kelp) and *D. willana* (Fig. 2a) are anchored by a fleshy non-calcified holdfast to coralline encrusted rocky surfaces in the lower intertidal zone (Adams, 1994; Nelson, 2013), and holdfasts extend subtidally by 1–2 m. Individual plants have fronds 3–5 m in length that typically drape down from the intertidal zone to depths of ∼ 5 m (Adams, 1994; Nelson, 2013). On sites exposed to higher wave action, holdfasts of *Durvillaea* may appear higher in the intertidal zone due to increased wave wash (Marsden, 1985); however, in sheltered areas and sites where waves are baffled holdfasts may be subaerially exposed at spring low tides but not at neap low tides (Sharyn Goldstien, personal communication, 2017). By contrast, *Carpophyllum* is only present in the low intertidal zone where it forms a distinct band close to low water (Nelson, 2013) (label C in Fig. 2c) and is not normally emergent at low spring tides (Sharyn Goldstien, personal communication, 2017). Although both *Carpophyllum* and *Durvillaea* may be present on open coasts (Fig. 2a), *Durvillaea* dominates in exposed sites, and *Carpophyllum* is more abundant at relatively sheltered locations. Dead stranded and living representatives of one or both of these brown algae were present at all the rocky coastal sites visited in this study, making *Carpophyllum* and *Durvillaea* an excellent combination of biozone markers for measuring coseismic uplift.

The reproductive season for *Durvillaea* is during the winter months, peaking in August, and harvesting studies have shown slow resettlement when fronds are removed in September through February (Hay and South, 1979). The intertidal zone on the Kaikōura coast is undergoing recovery from the November 2016 earthquake, and stabilised intertidal zones are not yet re-established. In temperate climate settings this may take several years, as shown by Castilla and Oliva (1990) following the 1985 Chile earthquake.

3 Methods

To measure coseismic uplift due to the Kaikōura earthquake, independent methods utilising marine biological sea level indicators, tidal gauge measurements, remote sensing techniques (RTK GNSS and lidar) and strong-motion recordings are used. The characteristics of each dataset collected and the methodology used to derive tectonic uplift are presented below. All uplift data are available in the Supplement.

3.1 Kaikōura tide gauge

New Zealand has 15 tide gauges which record tidal variation, tsunami events, eustatic sea level changes and vertical displacements of the coast. The Kaikōura tide gauge (Fig. 1) measures sea level relative to two Druck PTX1830 sensors (KAIT 40 and 41, each referenced to different datums) located at the end of the wharf at Kaikōura (WGS 84: −42.41288, 173.70277°; NZTM: 1657824, 5304141). In this study, data from the KAIT 41 sensor (http://apps.linz.govt.nz/ftp/sea_level_data/KAIT/, last access: 5 February 2017) are used exclusively to maintain internal consistency, although results would be the same had KAIT 40 been used. The instrument is fixed to bedrock beneath the wharf; it is referenced to nearby benchmarks, including one on the wharf itself (LINZ geodetic code EEFL), and records sea level at 1 min intervals. The data are recorded in UTC and the water levels represent water surface elevation above the base of the tide gauge in metres. The tide gauge was established in late May 2010 and operated continuously through the period of the 14 November Kaikōura earthquake, recording tectonic uplift at the site. KAIT 41 tide-gauge data assembled for this study spanned the period from 1 December 2015 to 7 February 2017 and indicate that tidal range varies between a spring tide average of ca. 2 and ca. 1.25 m during neap tides (Table 1). Spring low tides before the Kaikōura earthquake registered ca. 2.05 m on the gauge, while spring high tides were ca. 4.05 m. After the earthquake, low-water spring tide measured ca. 1.1 m and high-water spring ca. 3.1 m. Neap tides measured ca. 2.5 m (low) and ca. 3.7 m (high) before the earthquake and ca. 1.5 m (low) and ca. 2.75 m (high) after the earthquake (Table 1).

To determine the absolute uplift value from the tide-gauge data (U_{TG}; see File S1 in the Supplement) we used the following methodology: (A) subtracted the high spring and high neap tide readings before the earthquake from those after the earthquake; (B) averaged high-tide and low-tide readings from several tidal cycles (3 d period) before and after the earthquake; (C) aligned pre-earthquake tidal data with post-earthquake data and incrementally adjusted them until achieving a best fit; (D) compared the average water elevation from a pre-earthquake month to the same month's data after the earthquake (e.g. December 2015 against December 2016); and (E) calculated the difference in average waterline elevations for an extended period (44 d) before and after the earthquake (30 October to 27 December). The average uplift (U_{TG}) estimated from the above steps (Tables 1 and 2) is subsequently used to independently estimate the pre-earthquake upper range of the species used in this study
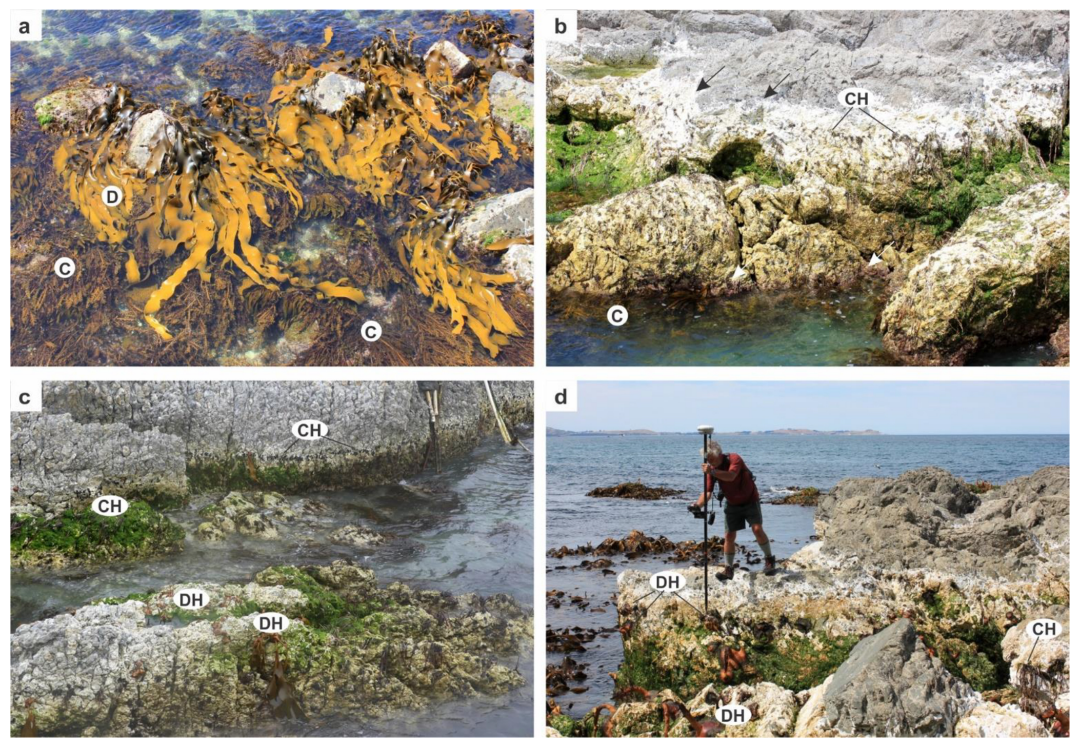
Figure 2. Field photographs of the intertidal zone and biota near Kaikōura (taken after the earthquake). **(a)** Healthy *Durvillaea* (mostly *D. willana*) (D) and *Carpophyllum* (C) photographed at low tide. **(b)** Uplifted bedrock north of Paia Point showing living *Carpophyllum* (C) and dead *Carpophyllum* holdfast stumps (CH). Also note the living pink coralline algae at the waterline and bleached morbid coralline algae (arrows) and bright green *Ulva*. **(c)** Uplifted intertidal zone near the Kaikōura tide gauge, showing a distinctive line of *Carpophyllum* holdfasts (CH) and dispersed *Durvillaea* holdfasts (DH). **(d)** Uplifted intertidal zone near Paia Point. One of the authors (John Begg) is measuring the elevation of *Durvillaea* holdfasts (DH) and *Carpophyllum* holdfasts (CH) using RTK GNSS survey equipment. Note the distinctive white zone of dead coralline algae.

Table 1. Calculation of uplift at the Kaikōura tide gauge (KAIT) using tide-gauge readings for high and low spring tides as well as high and low neap tides (see Sect. 3.1). Mean uplift is indicated in bold, derived by averaging the neap and spring low- and high-tide offsets.

	Spring tide		Neap tide		Uplift	
	Pre-EQ	Post-EQ	Pre-EQ	Post-EQ	Spring diff.	Neap diff.
High tide	4.05 m	3.1 m	3.7 m	2.75 m	0.95 m	0.95 m
Low tide	2.05 m	1.1 m	2.5 m	1.5 m	0.95 m	1 m
Range	2 m	2 m	1.2 m	1.25 m	**Mean diff.**	**0.96 m**

(see Sect. 3.2). It has also acted as a reference point against which all other instrumental and handheld measurements are compared.

Some limitations on calculating vertical displacement from tide-gauge records arise from the specific circumstances associated with the record around the 14 November 2016 $M_w = 7.8$ Kaikōura earthquake. This event struck during a period of sharply increasing tidal change due to high spring tides (related to lunar perigee and approaching solar perihelion) that culminated a few days after the earthquake. In addition, the earthquake generated a significant tsunami (Power et al., 2017), the effects of which persist in

the tide-gauge record for at least 12 h after the earthquake. Further, a day after the earthquake, Kaikōura was subjected to a southerly storm with powerful swells, and these are also apparent in the tide-gauge data. These factors result in some blurring in the precision of uplift deriving from the difference between pre-earthquake and post-earthquake data.

Uplift values calculated from tide-gauge data were compared with those derived from lidar differencing data (see Sect. 3.4.1). Biological data from this site (see Sect. 3.2) were used to calibrate the elevation of the upper extent of brown algal holdfasts relative to sea level (in this case, MLWS).

Table 2. Absolute uplift values calculated from the Kaikōura tide-gauge data using methods B–E. Method B: comparison of average high-tide and low-tide readings from several tidal cycles (3 d period) before and after the earthquake. Method C: aligning pre-earthquake tidal data with post-earthquake data and incrementally adjusting them until a best fit. Method D: comparing the average water elevation from a pre-earthquake month to the same month's data after the earthquake (December 2015 against December 2016). Method E: calculating the difference in average waterline elevations for an extended period (44 d) before and after the earthquake (14 November to 27 December). For Method A, we refer to the methodology established in Sect. 3.1 and presented in Table 1. The overall mean uplift, UTG and standard deviation are shown in bold and are calculated by summing mean uplift values from each method and dividing by the number of methods.

Method	Data points	Mean uplift (m)
A		0.96
B	6	0.95
C	17 568	0.98
D	44 640	0.96
E	17 932	0.97
Overall mean uplift U$_{TG}$		**0.96**
Standard deviation		**0.02**

3.2 Biological data collection

Biological data collected comprised the location and elevation of approximately 400 stranded algal holdfasts during a 10 d period approximately 2.5 months after the Kaikōura earthquake (File S2). The decay of attached and uplifted biota was well advanced, and, in most cases, the uplifted remnants of marine algae, our primary target species, were restricted to holdfast stumps of *Durvillaea* or *Carpophyllum* with brittle fronds attached (Fig. 2b–d). Despite the decay of algae, the position of the remaining stumps clearly reflected pre-earthquake algae distribution evidenced by a lack of rock "scarring" whereby removed stumps might also remove other intertidal biota and often expose fresh rock surfaces. The biological data presented in this paper were collected close to the Kaikōura tide gauge on the northern side of the peninsula, Kaikōura Harbour on the south side and from two localities along the south Kaikōura coastline: Paia Point and Omihi Point (Fig. 1).
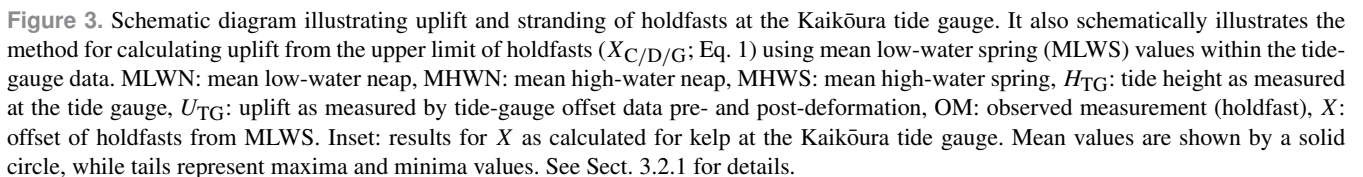
At all localities uplift was apparent from the exposure and subsequent degradation of intertidal biota, with algal holdfasts exposed above the waterline, and measurements were collected on rising or falling mid-tides and low tides. Holdfasts were preferentially measured on rock faces sheltered from, but retaining a connection to, the open sea to minimise error introduction by the potentially higher tidal position of *Durvillaea* in wave-washed sites. Each site was visually assessed to establish the upper extent of holdfasts, and the up-

per holdfasts were measured (as they represent specimens closest to the pre-earthquake upper limit for each species). In sites with boulders rather than bedrock exposure, only boulders showing that a portion of their surface was clearly within the pre-earthquake middle or upper tidal zone (evidenced by bare or barnacle-encrusted surfaces) and that had clearly remained undisturbed by strong ground shaking and subsequent storm wave exposure were selected for measurement, therefore ensuring that the upper limit of holdfasts was represented.

Two different methods were used to measure the vertically displaced biota. The primary method of collection of field data was by a real-time kinematic global navigation satellite system (RTK GNSS). At each site the water level was measured in the most sheltered area available to minimise wave effects, and the time the measurement was collected was recorded. Following measurement of the waterline, up to 20 holdfasts (either or both *Carpophyllum* and *Durvillaea*) were measured within close proximity. Where additional holdfasts were available at each site, the water level was remeasured and further sets of up to 20 holdfasts measured. This RTK collection method did not require the waterline measurement site and the holdfasts to be immediately adjacent to each other. Additional biological data were collected using a second method: direct tape measurement of the height of holdfasts above the water level. Tape measurements were collected between the waterline (measured between wavelet peaks and troughs) and the upper algal holdfasts on rock surfaces. Sheltered faces were again preferentially measured, although the requirement to have stranded holdfasts immediately adjacent to a measurable waterline meant that sites exposed to wave wash were more commonly used to achieve approximately 20 measurements. Each reading for both methods (RTK or tape) was annotated with the alga species measured, relative site exposure (exposed or sheltered) and the time of measurement.

3.3 Biological data processing

These field measurements of holdfast heights were then processed to determine coseismic uplift, taking into account the time of data measurement within the tidal cycle and the pre-earthquake living position of algal holdfasts. Three different methods were used for calculating tectonic uplift from the vertical offsets of the biological horizons. These were (a) tide-gauge calibration, (b) NIWA Tide Forecaster measurement and (c) LINZ tide prediction charts. The first method utilised data from the Kaikōura tide gauge and differs significantly from the two tide prediction methods by calibration to real-time water-level records of the Kaikōura tide gauge. The NIWA Forecaster and LINZ tidal chart methods are included, however, to simulate locations where real-time tide gauges are not available. All data and calculations are presented in File S2.

Figure 3. Schematic diagram illustrating uplift and stranding of holdfasts at the Kaikōura tide gauge. It also schematically illustrates the method for calculating uplift from the upper limit of holdfasts ($X_{C/D/G}$; Eq. 1) using mean low-water spring (MLWS) values within the tide-gauge data. MLWN: mean low-water neap, MHWN: mean high-water neap, MHWS: mean high-water spring, H_{TG}: tide height as measured at the tide gauge, U_{TG}: uplift as measured by tide-gauge offset data pre- and post-deformation, OM: observed measurement (holdfast), X: offset of holdfasts from MLWS. Inset: results for X as calculated for kelp at the Kaikōura tide gauge. Mean values are shown by a solid circle, while tails represent maxima and minima values. See Sect. 3.2.1 for details.

3.3.1 Deriving an upper living-position correction using the Kaikōura tide gauge ($X_{C/D/G}$)

This new method determines an upper living position for each species using the measured elevations of the stranded holdfasts and then relating them to the pre-earthquake tidal cycle (Fig. 3) by subtracting uplift recorded by the tide gauge. This enables the elevation of the holdfasts, which are being used to determine surface uplift, to be referenced to a pre-earthquake datum, in this case the base of the tidal cycle mean low-water spring (MLWS). The Kaikōura tide gauge provides a record of the pre- and post-earthquake MLWS. First the height of the stranded holdfast is determined by adding the waterline height measured in the tide gauge (H) and the observed height of the holdfast above the waterline in sheltered locations (OM). The offset of MLWS pre- and post-earthquake in the tide gauge calculated as uplift is sub-

tracted, along with the height of MLWS in the tide gauge. This leaves a residual height that reflects the pre-earthquake elevation of holdfasts of each species with respect to MLWS.

The upper holdfast living position is described here by the correction $X_{C/D}$, which is treated as a constant for *Carpophyllum* (X_C), *Durvillaea* (X_D) or a combination of both (X_G). $X_{C/D/G}$ was determined by Eq. (1):

$$X_{C/D/G} = (H_{TG} + OM_{C/D/G}) - U_{TG} - MLWS, \qquad (1)$$

where H_{TG} is the waterline height at the tide gauge at the time of data collection (which can be accessed from http://www.linz.govt.nz/ (last access: 17 August 2017) and which was averaged here over 10 min intervals to mitigate local fluctuations). $OM_{C/D/G}$ is the observed height above the waterline for each stranded holdfast (determined by subtracting the RTK waterline height measurement from each RTK holdfast measurement per site or directly using tape measurements; the subscripts C, D and G correspond to measurements for the different holdfasts). MLWS is the average tide-gauge reading for mean low-water spring tide (1.1 m for KAIT 41; see Table 1), and U_{TG} is this uplift calculated at the tide gauge by the method described in Sect. 3.1.

As *Carpophyllum* and *Durvillaea* occupy slightly different upper living positions in the intertidal zone, $X_{C/D}$ was calculated separately for each species. A general correction, X_G, using both *Carpophyllum* and *Durvillaea* holdfasts was also determined, to be applied at sites where holdfast species were not known or determined or where insufficient numbers of each were available and data were pooled by necessity. To calculate the correction, data were pooled by species irrespective of site. The method described here uses the upper extent of intertidal algae as marker horizons, as at Kaikōura these are readily available attached biota. However, biozone boundaries for any attached intertidal organism with a restricted tidal range could be used to calculate this correction factor.

3.3.2 Deriving tectonic uplift using the Kaikōura tide-gauge method ($U_{B(TG)}$)

Once the $X_{C/D/G}$ correction was derived as described above, coseismic uplift was calculated from biological data pooled by site in the location studied using Eq. (2):

$$U_{B(TG)} = ((H_{TG} + OM_{C/D/G}) - MLWS) - X_{C/D/G}, \qquad (2)$$

where $U_{B(TG)}$ is the uplift calculated from biological data at the Kaikōura tide gauge.

3.3.3 Deriving tectonic uplift using the NIWA Tide Forecaster ($U_{B(NIWA)}$)

In order to calculate uplift from sites distant from the tide gauge, RTK biological data were used in conjunction with tidal charts (https://www.niwa.co.nz/services/

online-services/tide-forecaster, last access: 5 March 2017) that provide tidal predictions for sites between formal chart stations and attempt to account for local variation. For this calculation, Eq. (3) is used:

$$U_{B(NIWA)} = (H_{NIWA} + OM_{C/D/G}) - X_{C/D\_NIWA}, \qquad (3)$$

where $OM_{C/D/G}$ is the observed elevation of the holdfasts relative to locally measured sea level, H_{NIWA} is the predicted tide height from NIWA charts at the survey time, and X_{C/D_NIWA} is a correction value (NIWA-Forecaster-calibrated correction) estimated to reflect the relative height of *Carpophyllum* and *Durvillaea* within the tidal cycle (Fig. 4). This value for X is independent of tidal gauge data as used above and relies on the assessment of qualitative biological data only. As described in Sect. 2.2, *Carpophyllum* in sheltered areas with a connection to the sea will not usually be exposed at low spring tide (LST) (Sharyn Goldstien, personal communication, 2017). Tidal prediction charts over 1 year were qualitatively assessed, and a mean low spring tide height of 0.1 m (X_{C_NIWA}) was estimated for the upper limit of *Carpophyllum* and used as the correction value for this species in data processing. Likewise, *Durvillaea* will be regularly exposed at low spring tides but usually not exposed at low neap tide (Sharyn Goldstien, personal communication, 2017). A correction (X_{D_NIWA}) of 0.25 m was estimated, representing a height between spring and neap low tides, relevant to the Kaikōura region. These values for X_{C/D_NIWA} assume that the upper holdfast elevations of *Carpophyllum* and *Durvillaea* are consistent between sheltered and exposed areas.

The value of H_{NIWA} was determined using the predicted tide heights and times from the NIWA Tide Forecaster website. The NIWA Tide Forecaster provides tide height at user-designated locations that may be between the fixed LINZ locations in order to accommodate the passage of tidal highs and lows between fixed points. H_{NIWA} was calculated using the following equation (Eq. 4) from http://www.linz.govt.nz/ (last access: 5 March 2017):

$$H_{NIWA} = h_1 + (h_2 - h_1)[(\cos A + 1)/2], \qquad (4)$$

where $A = \pi([(t - t_1)/(t_2 - t_1)] + 1)$ radians, t_1 and h_1 denote the time and height of the tide (high or low) immediately preceding time t, and t_2 and h_2 denote the time and height of the tide (high or low) immediately following time t. Only time t is measured; t_1, t_2, h_1 and h_2 are derived from predictive tide charts.

3.3.4 Process to derive tectonic uplift using the LINZ tide prediction charts ($U_{B(LINZ)}$)

Land Information New Zealand (LINZ) tide charts available at http://www.linz.govt.nz/ (last access: 5 March 2017) provide fixed tide prediction charts for New Zealand primary and secondary ports and were also used to derive H_{LINZ} using Eq. (3) as well as LINZ calibration correction values of
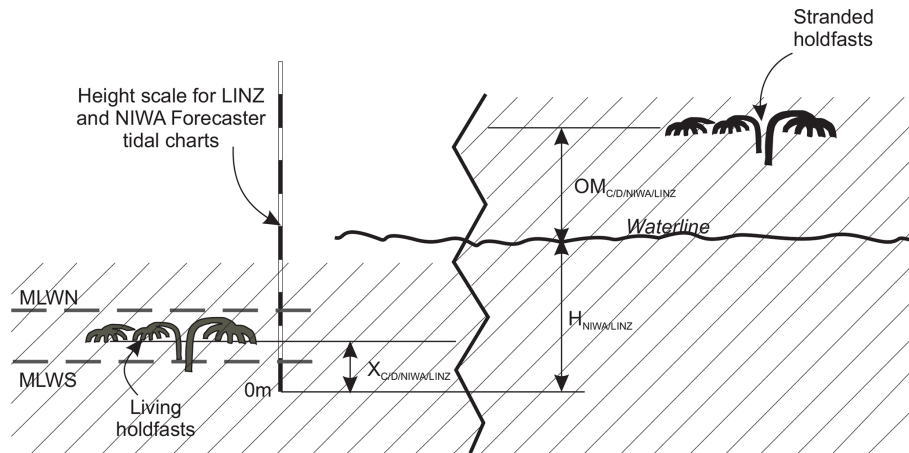
Figure 4. Schematic diagram illustrating the uplift and stranding of holdfasts used to calculate the offset of holdfasts ($X_{\mathrm{NIWA/LINZ}}$) from mean low-water spring (MLWS) independent from tide-gauge data. MLWN: mean low-water neap. Here MLWS is determined from LINZ and NIWA predictive charts, and the position of holdfasts with respect to MLWS and MLWN is determined from local knowledge of kelp distribution (Sharyn Goldstien, personal communication, 2017).

0.2 m for $X_{\mathrm{C\_LINZ}}$ and 0.4 m for $X_{\mathrm{D\_LINZ}}$ estimated as above from these charts. H_{LINZ} was again determined by Eq. (4) defined above, and only RTK data were processed this way.

3.3.5 Sources of error

Data points collected by RTK GNSS were accurate to ± 5 cm, and this applies to both the waterline measurement at each site and each holdfast measurement. Both of these measurements were used to derive OM, with a total error of ± 10 cm. Manually collected biological data rely on the accuracy of the waterline measurement taken. While sheltered microsites were selected for these measurements, they were placed at an estimated median water level between wavelets. This error is more pronounced when measuring waterline heights at more exposed sites. Additionally, the time at which the measurement was taken may have occurred when the water level was at either a positive or negative fluctuation from tidal prediction charts or tide-gauge readings for sites south of Kaikōura. The total error is difficult to quantify; however, an assessment of the Kaikōura tide-gauge data shows water-level fluctuations of less than ± 0.1 m. Averaging tide-gauge data over 10 min helped mitigate the error resulting from the tide gauge itself; however, the error introduced by sea level fluctuations away from the tide gauge remained.

Durvillaea lives along open coasts, but at very exposed sites pre-earthquake holdfasts would have sat higher than average in response to increased wave wash and run-up. This potential error is difficult to quantify as deviation from average heights will be linked to wave heights and run-up at individual sites that may be modified following uplift. For this reason, the most exposed sites were avoided (where possible) and data were collected from sheltered locations.

3.4 Differential lidar and strong-motion uplift estimates

3.4.1 Differential lidar (U_{lidar})

Differential lidar has been developed along the coastal south Kaikōura region using pre-earthquake (DEM_Kaikōura_2012_1m) and post-earthquake (NZVD2016 and DEM_NZTA_1m) surveys of road and railway routes using a common geodetic datum for each survey. To minimise the impact of gravity-induced slope failures and horizontal tectonic displacement on sloping ground during the earthquake, the difference in the altitude of 1×1 pixels along the post-earthquake centreline of roads was used. Specifically, for the Omihi Point and Paia Point study localities (see Fig. 1) the nearby State Highway 1 was used, while for the Kaikōura tide-gauge study site, a section of the coastal road near the wharf that houses the gauge was used. The road sections that acted as a reference level have low relief (e.g. < 10 cm relief) and are wider than the horizontal displacements recorded during the earthquake; thus, neither lateral tectonic displacement nor gravitational processes should significantly impact the differential lidar measurements. Collectively, a total of 510 differential lidar points were collected and analysed (148 at the Kaikōura tide gauge, 152 points at Paia Point and 210 points at Omihi Point) (File S3). These data were used to produce mean uplift estimates of at each site with 2σ uncertainties of ± 0.06–0.18 m (Table 6). Differential lidar data were not available immediately adjacent to Kaikōura Harbour on the south side of the peninsula.

3.4.2 Strong motion (U_{SM})

A further independent instrumental uplift measurement was achieved by calculating the static vertical displace-

Table 3. Results for the calculation of the upper living-position $X_{C/D/G}$ relative to MLWS for holdfasts at the Kaikōura tide gauge. Note that only holdfasts of *Carpophyllum* and *Durvillaea* in sheltered locations were used to calculate this elevation.

	Mean	SD	Median	Max	Min
All holdfasts X_G	0.31 m	0.10 m	0.32 m	0.50 m	0.01 m
Carpophyllum X_C	0.26 m	0.09 m	0.26 m	0.43 m	0.01 m
Durvillaea X_D	0.38 m	0.07 m	0.39 m	0.50 m	0.19 m

ment recorded by the nearby strong-motion site KIKS (Fig. 1). The KIKS station is located 2.2 km south of the Kaikōura tide gauge (lat., long.: $-42.426°$ N, $173.682°$ E; NZTM: 1656161, 5302714; see Fig. 1) and operated by GeoNET. The Kinemetrics FBA-ES-T-BASALT 2420 sensor is located at 8 m of elevation on the concrete floor of a single-storey building at Kaikōura Harbour. Ground acceleration is recorded with a period of 0.005 s and data can be downloaded online from ftp://ftp.geonet.org.nz/strong/processed/ (last access: 5 March 2017).

Static displacement was calculated from the vertical component of the instrument following the method of Wang et al. (2011) and using their software package *smbloc*, which applies an empirical baseline correction to remove linear pre- and post-event trends in the data. Static displacement derived with this method after large earthquakes has been shown to be robust (e.g. Schurr et al., 2012). Here, the resulting vertical displacement for the KIKS strong-motion station is 0.87 ± 0.06 m (see Table 6 and File S4 for further details on data processing).

4 Results and comparison of methods

4.1 Kaikōura tide-gauge locality

Tide-gauge data indicate that the Kaikōura tide gauge was coseismically uplifted by 0.96 ± 0.02 m (U_{TG}) (Tables 1 and 2) (see Sect. 3.1) and represents a key reference point for this study. In addition to providing an independent estimate of uplift, the tide-gauge data have been used to calculate the upper living-position correction factor $X_{C/D/G}$ from all stranded biological holdfast data collected proximal to the tide gauge (Eq. 1) (Table 3; Fig. 5).

The calculated corrections $X_{C/D}$ (Table 3) were applied to biological measurements collected proximal to the Kaikōura tide gauge (Fig. 5) and compared with uplift of the Kaikōura tide gauge (calculated in Sect. 3.1). RTK GNSS survey data of *Durvillaea* and *Carpophyllum* for sheltered and exposed holdfasts produce tectonic uplift values of 0.71 to 1.13 m, with a mean of 0.97 ± 0.08 m (Table 4, Fig. 5). Similarly, for all tape-measure data collected proximal to the tide gauge, tectonic uplift estimates range between 0.87 and 1.35 m, with a mean of 1.05 ± 0.11 (Table 4, Fig. 5). The resulting analysis suggests that *Carpophyllum* at sheltered sites recorded

Table 4. Comparison of uplift results for data collected by RTK and tape measure at the tide gauge, including a comparison of kelp types in both sheltered and exposed locations. Results are presented by holdfast species and exposure ranking independently of the collection site.

	Mean (m)	SD (m)	Min (m)	Max (m)
RTK data				
All data	0.97	0.08	0.71	1.13
Carpophyllum sheltered	0.96	0.09	0.71	1.13
Durvillaea sheltered	0.98	0.07	0.78	1.09
Tape-measure data				
All data	1.05	0.11	0.87	1.35
Carpophyllum sheltered	0.98	0.06	0.87	1.13
Carpophyllum exposed	1.06	0.07	0.92	1.22
Durvillaea sheltered	1.10	0.13	0.91	1.35
Durvillaea exposed	1.21	0.09	1.07	1.35

using an RTK GNSS and a tape measure produce uplift estimates that are, within the uncertainties given, indistinguishable from uplift recorded by the tide gauge (0.96 m) and differential lidar (0.92 cm) (Fig. 5). By contrast, estimates of uplift using *Durvillaea* are always higher than tide-gauge and differential lidar values. Tape measurements of *Durvillaea* produced the highest biological uplift estimates with exposed *Durvillaea* recording a mean uplift of 1.21 m, which is 0.25–0.29 m above the tide-gauge and differential lidar values (Table 4, Fig. 5). These data suggest that *Durvillaea* should be regarded as providing maximum uplift estimates, supporting previous work in suggesting that *Durvillaea* at exposed sites should be used with caution (e.g. Clark et al., 2017).

The same biological data collected near the Kaikōura tide gauge were then grouped by data collection location (sets of approximately 20 data points) rather than holdfast type, and uplift estimates produced results of 0.99 m ± 0.07 m, 0.92 m ± 0.10 m and 0.98 m ± 0.07 m, while tape measures resulted in uplift estimates of 1.00 m ± 0.07 m, 1.12 m ± 0.11 m and 1.19 m ± 0.08 m, respectively (Fig. 6a, Table 5). In addition to directly measuring water levels at the tide gauge, the NIWA Forecaster and LINZ tide charts were used to calculate uplift in an effort to test the utility of tide charts at remote locations where tide-gauge and instrument data may not be available. These comparisons are illustrated in Table 5 and Fig. 6. At the tide-gauge site, the LINZ tide chart produced, for *Carpophyllum*, uplift results 0.11–0.12 m greater than the tide-gauge method, while an NIWA Forecaster chart produced uplift estimates of 0.04–0.05 m greater than the tide-gauge mean (Table 5). As was the case for the tide-gauge calibration method, *Durvillaea* produced the greatest uplift at the tide gauge using the tide-chart method, with average uplift values of 1.18 and 1.24 m. In summary, uplift estimates calculated from *Carpophyllum*
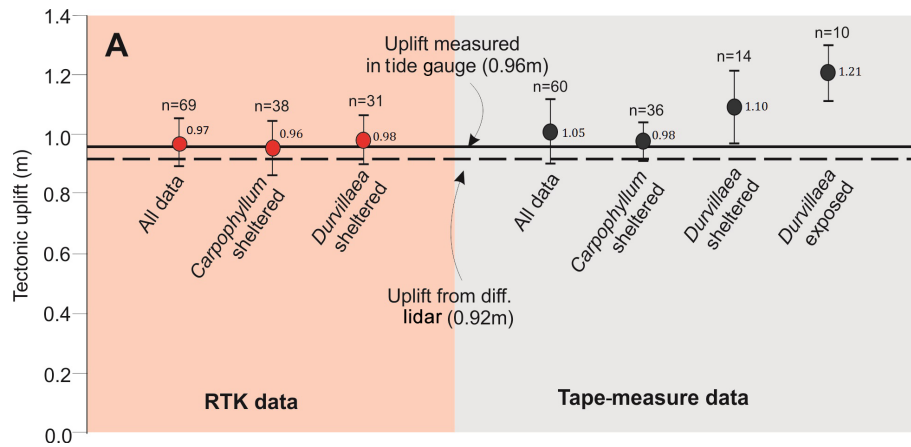
Figure 5. Uplift at the Kaikōura tide gauge calculated from the upper living positions of various kelp holdfasts and exposure sites plotted against the offset recorded at the same locality using the tide gauge and differential lidar. Holdfast data are presented as the mean and standard deviation, while the tide-gauge and lidar data are presented as the mean only. Black numbers beside the data points indicate the mean values, while *n* values at the top represent the number of measurements per category.

Table 5. Comparison of mean uplift values derived using RTK for the various methodologies (e.g. tide-gauge calibration method, NIWA Forecaster method, LINZ tide-chart method). As the source data remain identical for each method, the standard deviation reflects error derived from the RTK measurements. Data are presented by site at each location; when a site was sampled using both *Carpophyllum* and *Durvillaea*, the holdfast type is recorded as "mixed".

Site	Holdfast type	Tide-gauge mean (m)	NIWA Forecaster mean (m)	LINZ tide-chart mean (m)	SD* (m)
RTK					
Tide gauge 1	*Carpophyllum*	0.99	1.04	1.11	0.06
Tide gauge 2	*Carpophyllum*	0.92	0.97	1.04	0.10
Tide gauge 3	*Durvillaea*	0.98	1.18	1.24	0.07
Paia Point 1	*Carpophyllum*	1.27	1.27	1.24	0.11
Paia Point 2	*Durvillaea*	1.22	1.36	1.36	0.18
Paia Point 3	Mixed	1.18	1.17	1.12	0.16
Omihi Point 1	*Carpophyllum*	1.71	1.80	1.95	0.13
Kaikōura Hbr	*Carpophyllum*	0.74	0.85	0.98	0.12
Tape measure					
Tide gauge 1	*Carpophyllum*	1.00			0.07
Tide gauge 2	*Carpophyllum*	1.12			0.11
Tide gauge 3	*Durvillaea*	1.19			0.08
Tide gauge 4	Mixed	0.99			0.06
Paia Point 1	Mixed	1.27			0.09
Paia Point 2	Mixed	1.23			0.09
Omihi Point 1	Mixed	1.66			0.17
Kaikōura Hbr	*Carpophyllum*	0.66			0.10
Kaikōura Hbr	*Carpophyllum*	0.67			0.06

holdfasts processed using the NIWA Forecaster tide charts (rather than LINZ charts) are the most similar to direct uplift of the tide gauge itself, to the tide-gauge biological results and to lidar (plus 0–0.25 m), promoting their use in circumstances in which a tide gauge is unavailable. LINZ tide-chart methods produced results within 0.32 m of other methods.

4.2 Kaikōura harbour, Paia Point and Omihi Point

To further test the utility of the Kaikōura calibration method and the other methods under consideration, algae uplift data were also processed from the Kaikōura Harbour, Paia Point and Omihi Point sites. Data from these locations are not as detailed as those collected at the tide-gauge study site itself, with the distinction between *Carpophyllum* and *Durvillaea* as well as sheltered and exposed areas not always available.

At Paia Point, uplift estimates from all data collection and processing methods range from 1.12 to 1.36 m, with a mean uplift of $1.24\,\text{m} \pm 0.16\,\text{m}$ (Table 5; Fig. 6). While the biological uplift results are internally consistent, on average they are about 0.2 m higher than the differential lidar average uplift at this site, which is $1.05\,\text{m} \pm 0.07\,\text{m}$ (Table 6; Fig. 7). This higher estimate for biological data cannot be attributed to differences in species of algae or measurement technique; however, shoreline exposure to wave action cannot be excluded as a factor. The role of shoreline exposure may only be resolved once the uplifted shoreline is recolonised with new *Carpophyllum* and *Durvillaea*. Algal uplift measurements collected at Omihi Point (Fig. 1) and processed using the tide-gauge calibration correction $X_{C/D}$ are within 0.07 m of one another and uplift recorded by differential lidar (Tables 5 and 6, Fig. 6). RTK measurements from Omihi Point processed using the NIWA Forecaster and LINZ tide-chart methods are 0.08 and 0.23 m, respectively, above tide-gauge-calibrated estimates. In summary, there is no systematic dif-
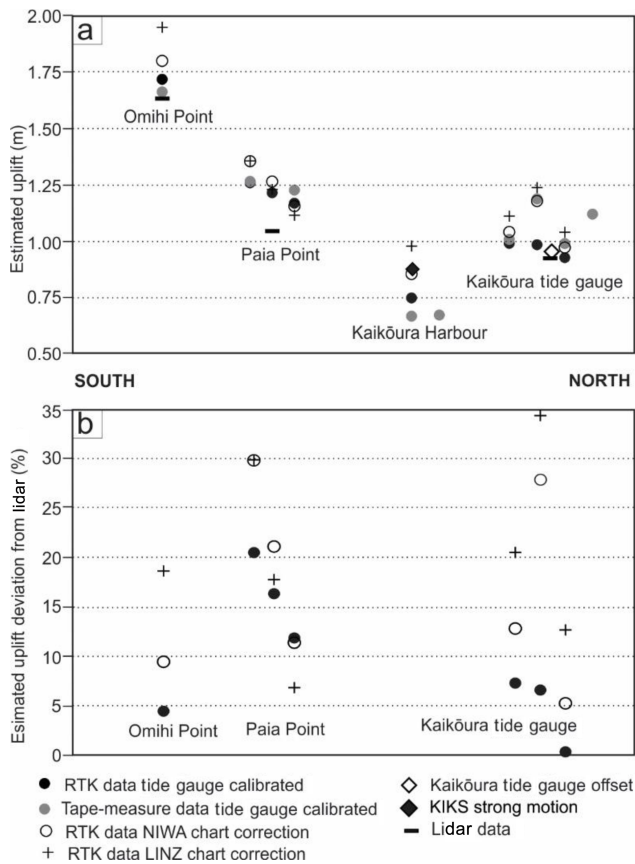
Figure 6. (a) Tectonic uplift in metres measured at the Kaikōura tide gauge, Kaikōura Harbour, Paia Point and Omihi Point from biological data processed using the tide-gauge correction, as well as NIWA and LINZ predictive tide-chart correction methods (see Sect. 3.2). These values are compared to uplift recorded by the tide gauge and differential lidar (where available). **(b)** Percentage of uplift deviation of the biological methods with respect to the lidar measurements. Horizontal axis not to scale.

ference in the uplift estimates at Paia Point and Omihi Point between the different measurement techniques (RTK GPS vs. tape measure), species of algae (*Carpophyllum* or *Durvillaea*) or tide charts (NIWA Forecaster or LINZ tide chart) (Fig. 6).

At the Kaikōura Harbour site, where the KIKS seismic station is located (Fig. 1), uplift estimates from biological data, processed with the tide-gauge-calibrated upper living-position methodology, are 0.74 m ± 0.12 m and 0.85 m ± 0.12 m for NIWA-calibrated methods and 0.98 m ± 0.12 m for LINZ methods. These results bracket the uplift result recorded by the strong-motion data of 0.87 m ± 0.06 m (Fig. 6). Differential lidar was not available adjacent to Kaikōura Harbour for comparison with biological measurements

Comparison of results for all biological methods, independent of location, shows a consistent correlation (Fig. 8). No single method stands out as producing persistently divergent

Table 6. Uplift calculated from differential lidar and strong-motion uplift estimated from the KIKS station.

|	Mean (m)	Median (m)	SD (m)	Max (m)	Min (m)
Differential lidar					
Tide gauge	0.92	0.91	0.06	1.13	0.77
Paia Point	1.05	1.05	0.07	1.31	0.90
Omihi Point	1.64	1.64	0.04	1.74	1.53
KIKS strong motion					
Kaikōura Harbour	0.87		0.06		

results from other methods, although all biological methods produce uplift estimates that are higher than lidar results. The tide-gauge-calibrated method has yielded results most consistent with lidar. At all sites uplift estimated using the tide-gauge calibration method give results within 0.0 to +0.21 m (or 0.35 % to 21 %) higher than lidar results, with a mean of +0.11 m (10 %). Further, at all sites and over all biological methods, uplifts estimates are 0.0 to +0.31 m (or < 34 %) higher than associated lidar results, with a mean of +0.17 m.

5 Discussion

The distribution of kelp within the intertidal zone at Kaikōura is well defined with respect to qualitative upper, middle and lower intertidal zones (Marsden, 1985). Nevertheless, because the width of the intertidal zone varies with site exposure, topography, wave wash and competition between different organisms, an attempt to quantify this uncertainty is made by calibrating coseismically uplifted intertidal brown algae (*Durvillaea* and *Carpophyllum*) in the immediate vicinity of the Kaikōura tide gauge, aiming to establish a quantitative correction value for the upper living position of the kelp holdfasts with respect to MLWS (Figs. 3 and 5).

Using Eq. (1) (see Sect. 3.2) at the Kaikōura tide gauge, an upper living-position correction of X_C of 0.26±0.09 m above MLWS is derived for sheltered *Carpophyllum maschalocarpum*. For *Durvillaea* in sheltered sites, the upper living-position correction X_D is 0.38±0.09 m above MLWS. These values were subsequently used to estimate tectonic uplift at sites located up to 15 km from the tide gauge and produced uplift measurements which were in good agreement with uplift calculated at the same localities by differential lidar (Figs. 6 and 7). Thus, it appears that this method of estimating correction values may be important as it provides, for the first time, an independent quantitative method for estimating the preferred upper living position for intertidal biota with respect to MLWS. This method may be applied elsewhere to other intertidal biota in the vicinity of a tide gauge. *Carpophyllum* is endemic to New Zealand, while *Durvillaea* is widespread in the Southern Hemisphere. The derived correc-
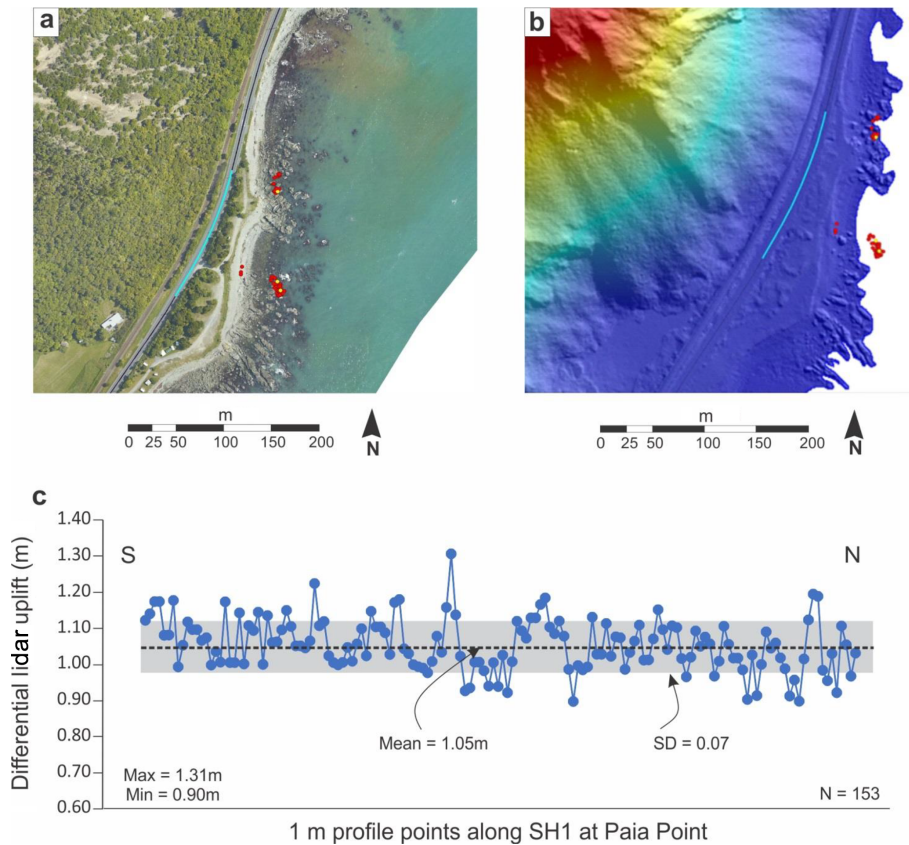
Figure 7. Locality, digital elevation imagery and differential lidar data for Paia Point (see Fig. 1 for location). **(a)** Aerial photo from Google Earth© imagery of Paia Point, State Highway 1 and uplift collection points. Blue line: portion of SH1 from which differential lidar uplift was calculated; red circles: RTK-GPS-collected kelp data points; yellow circles: tape-measure-collected kelp data points. **(b)** Digital elevation model developed from post-earthquake lidar data. Blue line and colour-coded circles as per **(a)**. **(c)** Plot of uplift of points at 1 m intervals along the blue line on SH1 in **(a)** and **(b)** derived from differential lidar.

tions are specific to these taxa in the Kaikōura region, which is characterised by a moderate tidal range. If these values are applied elsewhere, the uncertainty would be equal to the maximum correction value of 0.38 m. The three biological post-processing methods used to obtain uplift all yield results which are, within uncertainties, similar to one another, meaning that any of these methods could be applied depending on the available tidal data at the site of interest. Analysis of all data suggests that handheld measurements most often overestimate uplift compared to results from RTK GPS survey data.

In the vicinity of the Kaikōura tide gauge, biological results using the tide-gauge correction are most similar to non-biological methods. With increasing distance from the tide gauge, this new method provides reliable results; nevertheless, other biological methods were comparable. Progression of daily tides is even, and fluctuations from the expected tidal progression may occur over several minute intervals due to natural unevenness in the ocean surface caused by wind, barometric pressure and local topography (e.g. Garrison, 2010). While the influence of this natural fluctuation

for biological data collected proximal to the tide gauge is well mitigated by the use of the real-time tide-gauge water level (H), away from the Kaikōura tide gauge this real-time fluctuation is less able to be mitigated. Therefore, the NIWA and LINZ tidal chart calculations for H, and the associated corrections, may give equally accurate uplift estimates. Overall, the NIWA method produces results more consistent with non-biological methods than the LINZ method. Despite this, data collected by RTK and processed using predictive charts, such as LINZ, may be used to calculate uplift estimates and could be used with confidence in remote locations or locations where other methods are not available.

This study has shown that instrumental and biological methods can produce comparable results; yet, in order to reduce uncertainty in the biological methods, the biota should have a living position relative to an appropriate sea level datum that is calibrated against real-time tide-gauge data. To this end, our study has provided a new calibration method to derive a correction for this upper living position that can be applied globally where tide-gauge records are available. In circumstances in which tide-gauge records are unavail-
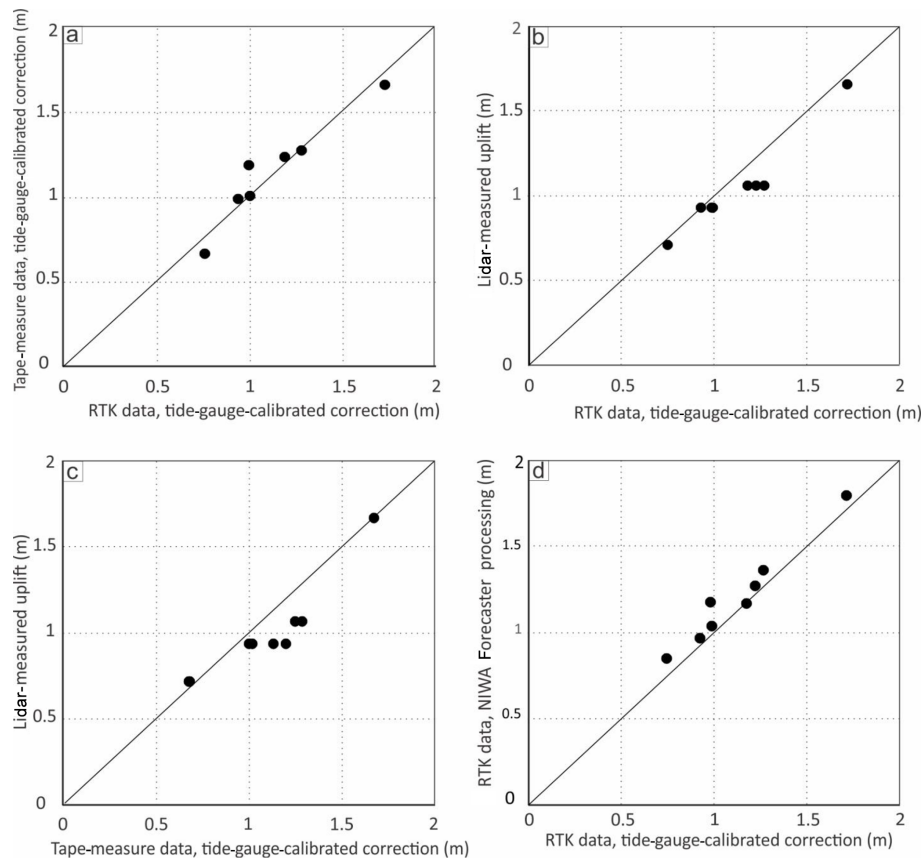
Figure 8. Cross plots of data collection and processing methods. **(a)** RTK and tape-measure uplift data processed using the tide-gauge correction method. **(b)** RTK uplift data, processed using the tide-gauge correction method, plotted against differential lidar uplift data. **(c)** Tape-measure uplift data, processed using the tide-gauge correction method, plotted against differential lidar uplift data. **(d)** RTK uplift data, processed using the tide-gauge correction method, plotted against the NIWA Forecaster tide-chart correction method.

able, the usage of predictive charts to process biological data may still be appropriate, accepting that uncertainties may be higher. The use of strongly anchored taxa such as algae may allow data to be gathered either immediately or during a period of time after deformation. The timeframe over which data could be recovered post-deformation will depend on local conditions, seasons and the anchoring strength of the taxa utilised.

6　Conclusions

Tectonic deformation determined from uplifted intertidal biozone indicators produces results comparable with tectonic uplift recorded by the Kaikōura tide gauge, remote sensing datasets (lidar and RTK GPS) and strong-motion seismic data. Calibrating measured intertidal biological data to real-time tide-gauge records gives results within an average of 0.11 m of those derived from direct uplift of the tide gauge and localised differential lidar values. Uplift results from biological data, calibrated using predictive tidal charts, are as reliable as other biological and non-biological methods when

distant from real-time tide gauges and are appropriate for use where differential lidar or other real-time remote sensing datasets are not available. Results from this study indicate that *Carpophyllum*, an alga with a tightly defined upper intertidal limit, is the most reliable predictor of uplift at sheltered sites. *Durvillaea*, an alga with a less well-defined upper intertidal limit, is less reliable, especially when measured at exposed sites. Biological data collected by RTK GNSS give the strongest overall comparison to non-biological methods of estimating uplift. Data collected by tape measure may be reliable where sheltered sites are available but are likely to provide higher apparent uplift results in exposed locations, where intertidal biozone boundaries are blurred and elevated by wave fetch and exposure on sections of a rocky coastline.

References

Adams, N. M.: Seaweeds of New Zealand: an illustrated guide, Canterbury University Press, Christchurch, New Zealand, 1994.

Bodin, P. and Klinger, T.: Coastal uplift and mortality of intertidal organisms caused by the September 1985 Mexico earthquakes, Science, 233, 1071–1073, 1986.

Carver, G. A., Jayko, A. S., Valentine, D. W., and Li, W. H.: Coastal uplift associated with the 1992 Cape Mendocino earthquake, northern California, Geology, 22, 195–198, 1994.

Castilla, J. C.: Earthquake-caused coastal uplift and its effect on rocky intertidal kelp communities, Science, 242, 440–443, 1988.

Castilla, J. C. and Oliva, D.: Ecological consequences of coseismic uplift on the intertidal kelp belts of *Lessonia nigrescens* in central Chile, Estuar. Coast Shelf. Sci., 31, 45–56, 1990.

Castilla, J. C., Manríquez, P. H., and Camaño, A.: Effects of rocky shore coseismic uplift and the 2010 Chilean mega-earthquake on intertidal biomarker species, Mar. Ecol. Prog. Ser., 418, 17–23, 2010.

Cesca, S., Zhang, Y., Mouslopoulou, V., Wang, R., Saul, J., Savage, M., Heimann, S., Kufner, S.-K., Oncken, O., and Dahm, T.: Complex rupture process of the M_W 7.8, 2016, Kaikoura earthquake, New Zealand, and its aftershock sequence, Earth Planet. Sc.

Lett., 478, 110–120, https://doi.org/10.1016/j.epsl.2017.08.024, 2017.

Clark, K. J., Nissen, E. K., Howarth, J. D., Hamling, I. J., Mountjoy, J. J., Ries, W. F., Jones, K., Goldstien, S., Cochran, U. A., Villamor, P., Hreinsdóttir, S., Litchfield, N. J., Mueller, C., Berryman, K. R., and Strong, D. T.: Highly variable coastal deformation in the 2016 M_W 7.8 Kaikōura earthquake reflects rupture complexity along a transpressional plate boundary, Earth Planet. Sc. Lett., 474, 334–344, 2017.

De Mets, C. R., Gordon, R. G., Argus, D., and Stein, S.: Effect of recent revisions to the geomagnetic reversal time scale on estimates of current plate motions, Geophys. Res. Lett., 21, 2191–2194, 1994.

Eberhart-Phillips, D. and Bannister, S.: 3-D imaging of Marlborough, New Zealand, subducted plate and strike-slip fault systems, Geophys. J. Intern., 182, 73-96, 2010.

Farías, M., Vargas, G., Tassara, A., Carretier, S., Baize, S., Melnick, D., and Bataille, K.: Land-level changes produced by the M_W 8.8 2010 Chilean earthquake, Science, 329, 916, https://doi.org/10.1126/science.1192094, 2010.

Fitzroy, R.: Proceedings of the second expedition, 1831–1836: under the command of Captain Robert Fitzroy, in: Volume II of the narrative of the surveying voyages of His Majesty's ships Adventure and Beagle between Years 1826 and 1836, describing their examination of the southern shores of South America, and the Beagle's circumnavigation of the globe, Henry Colburn, London, UK, 1839.

Garrison, T.: Oceanography: An Invitation to Marine Science, 7th Edn., Thomson Learning, Brooks, Cole, 2010.

Graham, M.: An account of some effects of the late earthquakes in Chili. Extracted from a letter to Henry Warburton, Esq V.P.G.S, T. Geol. Soc. Lond., 2, 413–415, 1824.

Hamling, I. J., Hreinsdóttir, S., Clark, K., Elliott, J., Liang, C., Fielding, C., Litchfield, N., Villamor, P., Wallace, L., Wright, T. J., D'Anastasio, E., Bannister, S., Burbidge, D., Denys, P., Gentle, P., Howarth, J., Mueller, C., Palmer, N., Pearson, C., Power, W., Barnes, P., Barrell, D. J. A., Van Dissen, R., Langridge, R., Little, T., Nicol, A., Pettinga, J., and Rowland, J.: Complex multi-fault rupture during the 2016 M_W 7.8 Kaikōura earthquake, New Zealand, Science, 356, 6334, https://doi.org/10.1126/science.aam7194, 2017.

Hay, C. H. and South, G. R.: Experimental ecology with particular reference to proposed commercial harvesting of *Durvillaea* (Phaeophyta, Durvillaeales) in New Zealand, Bot. Mar., 22, 431–436, 1979.

Jaramillo, E., Melnick, D., Baez, J. C., Montecino, H., Lagos, N. A., Acuña, E., Manzano, M., and Camus, P. A.: Calibrating coseismic coastal land-level changes during the 2014 Iquique (M_W =.2 8) earthquake (northern Chile) with leveling, GPS and intertidal biota, PLoS ONE, 12, e0174348, https://doi.org/10.1371/journal.pone.0174348, 2017.

Kaiser, A., Balfour, N., Fry, B., Holden, C., Litchfield, N., Gerstenberger, M., D'Anastasio, E., Horspool, N., McVerry, G., Ristau, J., Bannister, S., Christophersen, A., Clark, K., Power, W., Rhoades, D., Massey, C., Hamling, I., Wallace, L., Mountjoy, J., Kaneko, Y., Benites, R., Van Houtte, C., Dellow, S., Wotherspoon, L., Elwood, K., and Gledhill, K.: The 2016 Kaikōura, New Zealand, Earthquake: Prelimi-

nary Seismological Report, Seismol. Res. Lett., 88, 727–739, https://doi.org/10.1785/0220170018, 2017.

Laborel, J. and Laborel-Deguen, F.: Biological indicators of relative sea-level variations and of co-seismic displacements in the Mediterranean region, J. Coast. Res., 10, 395–415, 1994.

Litchfield, N. J., Villamor, P., Dissen, R. J. V., Nicol, A., Barnes, P. M., Barrell, D. J. A., Pettinga, J. R., Langridge, R. M., Little, T. A., Mountjoy, J. J., Ries, W. F., Rowland, J., Fenton, C., Stirling, M. W., Kearse, J., Berryman, K. R., Cochran, U. A., Clark, K. J., Hemphill-Haley, M., Khajavi, N., Jones, K. E., Archibald, G., Upton, P., Asher, C., Benson, A., Cox, S. C., Gasston, C., Hale, D., Hall, B., Hatem, A. E., Heron, D. W., Howarth, J., Kane, T. J., Lamarche, G., Lawson, S., Lukovic, B., McColl, S. T., Madugo, C., Manousakis, J., Noble, D., Pedley, K., Sauer, K., Stahl, T., Strong, D. T., Townsend, D. B., Toy, V., Williams, J., Woelz, S., and Zinke, R.: Surface Fault Rupture from the M_w 7.8 2016 Kaikōura Earthquake, New Zealand, and Insights into Factors Controlling Multi-Fault Ruptures, Bull. Seismol. Soc. Am., 108, 1496–1520, https://doi.org/10.1785/0120170300, 2018.

Marsden, I. D.: Between the tides on the Kaikoura Peninsula, Mauri Ora, 12, 69–93, 1985.

Melnick, D., Cisternas, M., Moreno, M., and Norambuena, R.: Estimating coseismic coastal uplift with an intertidal mussel: calibration for the 2010 Maule Chile earthquake ($M_w = 8.8$), Quaternary Sci. Rev., 42, 29–42, 2012.

Mouslopoulou, V., Begg, J. G., Nicol, A., Oncken, O., and Prior, C.: Formation of Late Quaternary paleoshorelines in Crete, Eastern Mediterranean, Earth Planet. Sc. Lett., 431, 294–307, 2015a.

Mouslopoulou, V., Nicol, A., Begg, J., Oncken, O., and Moreno, M.: Clusters of mega-earthquakes on upper plate faults control the Eastern Mediterranean hazard, Geophys. Res. Lett., 42, 10282–10289, https://doi.org/10.1002/2015GL066371, 2015b.

Mouslopoulou, V., Saltogianni, V., Nicol, A., Oncken, O., Begg, J., Babeyko, A., Cesca, S., and Moreno, M.: Breaking a subduction-termination from top-to-bottom: the 2016 Kaikōura earthquake, Earth Planet. Sc. Lett., 506, 221–230, https://doi.org/10.1016/j.epsl.2018.10.020, 2019.

Nelson, W.: New Zealand Seaweeds; an Illustrated Guide, Te Papa Press, Wellington, New Zealand, 2013.

Nicol, A., Khajavi, N., Pettinga, J., Fenton, C., Stahl, T., Bannister, S., Pedley, K. L., Hyland-Brook, N., Bushell, T., and Hamling, I.: Preliminary geometry, slip and kinematics of fault ruptures during the 2016 M_W 7.8 Kaikōura Earthquake in the North Canterbury region of New Zealand, Bull. Seismol. Soc. Am., 108, 1521–1539, 2018.

Ortlieb, L., Barrientos, S., and Guzmán, N.: Coseismic coastal uplift and coralline algae record in Northern Chile: the 1995 Antofagasta earthquake case, Quaternary Sci. Rev., 15, 949–960, 1996.

Pirazzoli, P. A., Thommeret, J., Thommeret, Y., Laborel, J., and Montaggioni, L.: Crustal block movements from Holocene shorelines: Crete and Antikythira (Greece), Tectonophysics, 86, 27–43, 1982.

Pirazzoli, P. A., Delibrias, G., Kawana, T., and Yamaguchi, T.: The use of barnacles to measure and date relative sea-level changes in the Ryukyu Islands, Japan, Palaeogeogr. Palaeoecl., 49, 161–174, 1985.

Plafker, G.: Tectonic deformation associated with the 1964 Alaska earthquake, Science, 148, 1675–1687, 1965.

Plafker, G. and Ward, S. N.: Backarc thrust faulting and tectonic iplift along the Caribbean sea coast during the April 22, 1991 Costa Rica earthquake, Tectonics, 11, 709–718, 1992.

Pondard, N. and Barnes, P. M.: Structure and paleoearthquake records of active submarine faults, Cook Strait, New Zealand: Implications for fault interactions, stress loading, and seismic hazard, J. Geophys. Res., 115, B12320, https://doi.org/10.1029/2010JB007781, 2010.

Power, W., Clark, K., King, D. N., Borrero, J., Howarth, J., Lane, E. M., Goring, D., Goff, J., Chague-Goff, C., Williams, J., Reid, C., Whittaker, C., Mueller, C., Williams, S., Hughes, M., Hoyle, J., Bind, J., Strong, D. T., Litchfield, N., and Benson, A.: Tsunami runup and tide-gauge observations from the 14 November 2016 M7.8 Kaikōura earthquake, New Zealand, Pure Appl. Geophys., 174, 2457–2473, 2017.

Ramirez-Herrera, M.-T. and Orozco, J. J. Z.: Coastal uplift and mortality of coralline algae caused by a 6.3 M_w earthquake, Oaxaca, Mexico, J. Coast. Res., 18, 75–81, 2002.

Schurr, B., Asch, G., Rosenau, M., Wang, R., Oncken, O., Barrientos, S., Salazar, P., and Vilotte, J. P.: The 2007 M7.7 Tocopilla northern Chile earthquake sequence: Implications for along-strike and downdip rupture segmentation and megathrust frictional behaviour, J. Geophys. Res., 117, B05305, https://doi.org/10.1029/2011JB009030, 2012.

Stiros, S. C., Arnold, M., Pirazzoli, P. A., Laborel, J., Laborel, F., and Papageorgiou, S.: Historical coseismic uplift on Euboea Island, Greece, Earth Planet. Sc. Lett., 108, 109–117, 1992.

Vargas, G., Farías, M., Carretier, S., Tassara, A., Baize, S., and Melnick, D.: Coastal uplift and tsunami effects associated to the 2010 M_w 8.8 Maule earthquake in Central Chile, Andean Geol., 38, 219–238, 2011.

Wallace, L. M., Barnes, P., Beavan, R. J., Van Dissen, R. J., Litchfield, N. J., Mountjoy, J., Langridge, R. M., Lamarche, G., and Pondard, N.: The kinematics of a transition from subduction to strike-slip: an example from the central New Zealand plate boundary, J. Geophys. Res., 117, B02405, https://doi.org/10.1029/2011JB008640, 2012.

Wang, R., Schurr, B., Milkereit, C., Shao, Z., and Jin, M.: An improved automatic scheme for empirical baseline correction of digital strong-motion records, Bull. Seismol. Soc. Am., 101, 2029–2044, 2011.

Wesson, R. L.: Darwin's First Theory, Pegasus Books, New York, 2017.

Wesson, R. L., Melnick, D., Cisternas, M., Moreno, M., and Ely, L. L.: Vertical deformation through a complete seismic cycle at Isla Santa Maria, Chile, Nat. Geosci., 8, 547–551, 2015.